Available online at www.sciencedirect.com
SCIENCE DIRECT
International Journal of Heat and Mass Transfer 49 (2006) 3325–3337
International Journal of HEAT and MASS TRANSFER
www.elsevier.com/locate/ijhmt

Bias effects on heat transfer measurements in microchannel flows

Roland Bavière [a,b], Michel Favre-Marinet [a,*], Stéphane Le Person [a]

[a] Laboratoire des Ecoulements Géophysiques et Industriels, CNRS-UJF-INPG, 1025 rue de la Piscine, BP 53 X, 38041 Grenoble Cedex, France
[b] Centre de Recherches sur les Très Basses Températures, CNRS B.P. 166, 38042 Grenoble Cedex 09, France

Received 4 October 2005; received in revised form 20 February 2006
Available online 22 May 2006

Abstract

This work is devoted to both experimental and numerical investigations of the hydrodynamics and associated heat transfer in two-dimensional microchannels from 700 μm to 200 μm in height. The design of the test section enabled to vary the channel height and to set a quasi-constant heat flux at the microchannel surface. Laminar developing, transitional and turbulent regimes of water flows were explored ($200 < Re < 8000$). A significant decrease in the Nusselt number was observed in the laminar regime when the channel spacing was decreased while the Poiseuille number remained unchanged in regard to conventional channel flow. It is shown that a bias effect in the solid/fluid interface temperature measurements is most likely responsible for this scale effect. The temperature error was estimated and accounted for in the determination of the Nusselt number. The corrected values have been found to be consistent with the conventional laws both in the laminar and in the beginning of the turbulent regime.

Keywords: Microheat transfer; Microchannel; Temperature measurements

1. Introduction

The development of microscale systems has grown rapidly during last decades, making possible many applications. In the field of heat transfer, use of microchannels seems very promising for cooling electronic equipment. Enhancement of heat transfer coefficient is obviously expected with reduction of length scales, and this has been observed many times starting with the experiments of Tuckerman and Pease [1]. These practical advantages of microchannel heat sinks have stimulated a strong current of research from experimental, theoretical and also numerical points of view in the last 10 years. A comprehensive survey may be found in [2].

Until a recent period, experimental studies on microchannel hydrodynamics reported in the literature presented a strong dispersion of results [3,4] and sometimes disagreed with the conventional theories of transport phenomena which are well verified in macroscale flows. However, recent works have confirmed the classical laws of hydrodynamics for flows in microtubes with inner diameter higher [5,6] or smaller than 50 μm [7–9]. These recent papers seem to demonstrate that there is no special size effect on hydrodynamics for water flows in microchannels with characteristic dimensions down to the order of a few microns.

The situation is rather similar although more complicated for heat transfer in microchannels [10–16]. In 2001, Sobhan and Garimella [2] pointed out the dispersion of results published since 1984. They also listed many possible sources of error in interpreting experimental data (entrance effects, roughness effects, non-uniformity of channel dimensions, thermal and flow boundary conditions, uncertainties and errors in instrumentation). If we consider the laminar regime of liquid flows, several experimental studies found discrepancies between heat transfer in microchannels and that in channels of conventional size. Two different trends may be distinguished in these results:

* Corresponding author. Tel.: +33 4 76 82 50 49; fax: +33 4 76 82 52 71.
E-mail addresses: Roland.Baviere@grenoble.cnrs.fr (R. Bavière), Michel.Favre-Marinet@hmg.inpg.fr (M. Favre-Marinet), Stephane.Leperson@hmg.inpg.fr (S. Le Person).

0017-9310/$ - see front matter © 2006 Elsevier Ltd. All rights reserved.
doi:10.1016/j.ijheatmasstransfer.2006.03.014

Nomenclature

C_p	specific heat at constant pressure, J kg^{-1} K^{-1}
D_h	hydraulic diameter, m
e	microchannel spacing, m
e_s	length scale for longitudinal conduction, m
f	Fanning friction factor
h	convection heat transfer coefficient, W m^{-2} K^{-1}
ΔH	head loss, m
g	acceleration due to gravity, m s^{-2}
L	channel length, m
L^+	non-dimensional channel length
M	conduction parameter
Nu	Nusselt number
p	pressure, N m^{-2}
Δp	pressure drop between channel inlet/outlet, N m^{-2}
Po	Poiseuille number
Pr	Prandtl number
R	radius of quarter cylinder at channel entrance, m
Q_m	mass flow-rate, kg s^{-1}
Re	Reynolds number $= \rho V_b 2e/\mu$
T	temperature, K
ΔT	measurement error on temperature, K
$\vec{V}$	velocity vector, m s^{-1}
V_b	bulk velocity, m s^{-1}
x	abscissa along the channel, m
y	coordinate in the direction perpendicular to the channel walls, m
x^*	entrance region parameter (Eq. (3))
w	channel width, m

Greek symbols

λ	thermal conductivity, W m^{-1} K^{-1}
ρ	density, kg m^{-3}
μ	dynamic viscosity, kg m^{-1} s^{-1}
φ	heat flux, W m^{-2}
Φ	total heat flux, W
τ	averaged wall shear stress, N m^{-2}

Subscripts and abbreviations

c	critical
elec	electric
exp	experimental
f	fluid
film	average between interface and bulk temperatures
in	inlet
lam	laminar
num	numerical
out	outlet
s	solid
theo	theoretical
w	wall

(1) variation of the Nusselt number with the Reynolds number; and
(2) reduction in the Nusselt number with the microchannel size.

These two features may be observed in the results of Peng et al. [10], Celata et al. [12], Wu and Ping Cheng [14] and Reynaud et al. [15]. On the contrary, Qu et al. [11] and Gao et al. [13] found *Re*-independent but very low values of the Nusselt number (~1–2 in [11]). Tso and Mahulikar [16] observed that *Nu* decreased with increasing *Re* and argued that the very low values found for *Nu* resulted from dissipation effects. It must be underlined that experiments in microchannels are extremely difficult due to the small size of the test sections so that it is complicated to directly deduce the local Nusselt number from the measured quantities. As a result, several studies have relied on numerical modeling of the fluid flow and heat transfer to interpret experimental data. Some works [17–22] compared the results of numerical analysis to data published in the literature whereas other ones are experimental and numerical studies performed in the same group [11,23–26]. Research works have emphasized that among the possible sources of deviation from the conventional laws, effects of axial heat conduction in the walls and entrance effects in the microchannel test section have contributed to some of the observed deviations [22,27]. Recently, following Peterson [28], Maranzana et al. [29] underlined the growing importance of conduction effects with reduction in the microchannel size and Kroeker et al. [30] illustrated its consequences on the functioning of a heat sink with circular microchannels.

Previous experimental and numerical investigations conducted in our group [13,31] have revealed a significant reduction in the Nusselt number for microchannel spacing less than 500 μm which could not be attributed to the coupling of axial heat conduction in the walls with convection in the microchannel. This led us to perform further experiments in a test section similar to that of Gao et al. [13]. The experimental set-up is presented in the subsequent section. As outlined above, several assumptions are necessary to infer the heat exchange coefficient from the measured quantities. In particular, the heat flux distribution at the channel surface is needed. This point is addressed in Section 3 which presents a two-dimensional numerical simulation of the flow and heat transfer in a model similar to the actual test section. The experimental evolution of the Nusselt number in the microchannel is then presented and interpreted in Section 4.

2. Experimental set-up

In the experimental set-up, the active channel walls were two hand-polished plane brass blocks, separated by a stainless steel plate (of thickness e) with a hollowed out central part of width $w = 25$ mm (see Fig. 1). The blocks and a plate were assembled using bolts tightened at constant torque. This arrangement formed large-span channels 82 mm in length (parameter L) with walls in brass and an adiabatic 5 mm extra length in epoxy resin. The spacing e of the microchannel test section was determined by the plate thickness, which could be varied in the range [200 μm; 700 μm] by steps of 100 μm. Two sumps were machined in the blocks at channel inlet/outlet where pressure and temperature conditions were measured (p_{in}, p_{out}, T_{in}, T_{out}). The tested fluid was demineralized water with an electrical conductivity of 300 μS cm^{-1}. Details on the fluid loop, the characteristics of the sensors and the data acquisition system can be found in the paper of Gao et al. [13] and in [32]. Heating was provided by eight electric cartridges, which were inserted inside the blocks (see Fig. 1). The set-up was completely surrounded by epoxy resin insulation to prevent heat losses to the environment. Transversal slits were machined through the blocks and filled with molded epoxy resin in order to limit axial heat conduction during the experiments. The slits defined four compartments by block, each of them containing an electric cartridge and a thermocouple. This arrangement was aimed at adjusting a nearly uniform heat flux at the solid/fluid interface along the channel, thereby facilitating the interpretation of the experimental data. The heating length of the cartridges was chosen close to the channels width, hence allowing to neglect the transversal variations of temperature and heat flux in both the solid and fluid regions. Four thermocouples of type T (T1, T2, T3 and T4), 500 μm in diameter, were placed along the microchannel in the plane of symmetry of the test section (Fig. 1) for determining the temperature at the solid/fluid interface. T1 was located 5.5 mm downstream from the channel entrance and the others were placed every 20.5 mm apart. The thermocouples were inserted in blind holes 4 mm in diameter, which ended 500 μm away from the microchannel wall. Heat transfer grease was applied to all contact surfaces in order to reduce the thermal contact resistance and to improve temperature uniformity over the whole surface.

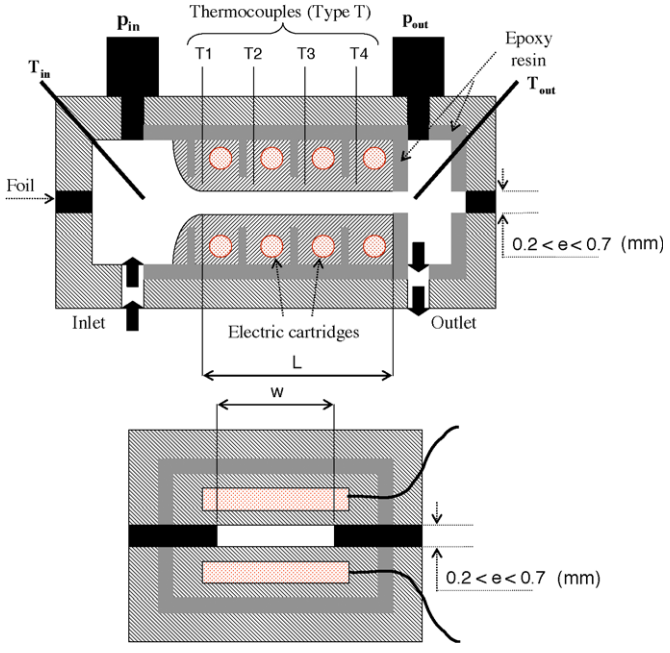

Fig. 1. Sketch of the test section. Top: longitudinal view (plane of symmetry); bottom: cross-sectional view.

The data were interpreted by using the Reynolds number Re and the Nusselt number Nu, both based on the hydraulic diameter D_h. The water properties, such as density (ρ), dynamic viscosity (μ), specific heat at constant pressure (C_p) and Pr number were determined at the average inlet/outlet temperature. The thermal conductivity λ_f used in Nu definition was determined at the local film temperature $T_{film} = \frac{T_w + T_f}{2}$ (average of wall and fluid bulk temperatures).

3. Numerical model

3.1. Computation domain, physical equations and boundary conditions

The geometry of the numerical model followed the details of the actual experimental set-up. Taking advantage of the large microchannel width to height ratio, we used a simplified two-dimensional model corresponding to the symmetry plane of the test section (Fig. 1). Calculations were performed for a channel height of $e = 500$ μm with fluid properties close to those of water. The model used the conventional mass, momentum and energy equations [33] along with the simplifying assumptions of laminar, steady and incompressible flow and negligible viscous dissipation effects. The resulting system of equations was the same as in [31].

The flow and energy equations were solved assuming respectively a uniform velocity and temperature profile at the upstream of the inlet sump and a fully developed condition at the channel exit plane. A constant energy source was set inside the cartridges reproducing the experimental total heat flux $\Phi = 180$ W. The model accounted for free convection heat transfer with surrounding air at the outside walls of the test section. The assumed values of the heat transfer coefficient and ambient temperature were equal to 10 W m^{-2} K^{-1} and 300 K, respectively.

3.2. Calculation and meshing

Numerical computations were carried out by using the commercial code Fluent 5.4. Details on the calculation procedure may be found in previous works performed in our group for a similar geometry [31,34]. Meshing of the model

was locally refined near the walls where normal gradients are important and in the channel entrance region because of the rapidly developing flow. The grid-convergence tests led us to use 1000 and 60 nodes in the channel length and height respectively. This arrangement resulted in a total of 2×10^5 cells for the complete computational domain. For $Re = 1491$, the level of normalized residuals for both velocity components reached 3×10^{-7} after 500 iterations and that corresponding to mass imbalance reached 2×10^{-4} after 100 iterations. The numerical solution obtained was found to be grid-independent.

3.3. Numerical results and discussion

It has already been outlined that conduction effects in the solid may influence the microchannel heat transfer. These effects may be quantified by the dimensionless parameter:

$$M = \frac{\lambda_s \frac{e_s}{L}}{\rho_f C p_f e V_b} \tag{1}$$

first proposed by Peterson [28] and used by Maranzana et al. [29] in a quasi-analytical computation of conjugated heat transfer in microchannels. M is the ratio of total heat flux longitudinally conducted in the walls to that convected by the stream. The transverse lengthscale for the conductive heat flux was chosen as the distance $e_s = 5$ mm from the bottom of the insulating transversal slits to the channel wall. Both the numerical simulations and the present experiments were conducted with moderate values of the Reynolds number Re leading to relatively low values of M. For the conditions of this study, M remained lower than 0.05. Thus, the coupling between convection in the microchannel and conduction in the walls was expected to be weak. This estimation is well confirmed by the numerical results. Fig. 2 presents the numerical wall heat flux φ_{num} along the channel, normalized by the value φ_{exp} corresponding to uniform distribution over the heating surface ($2Lw$), which was assumed during experiments. Comparison of the $Re = 431$ and 1994 cases suggests that this distribution is nearly insensitive to flow conditions. Fig. 2 shows that the heat flux distribution is sinusoidal-like due to the alternate arrangement of the electric heating cartridges and the insulation slits along the channel. However, the amplitude of the heat flux variations remains small over most of the channel length. The actual heat flux, as given by the numerical computations, may be replaced with a reasonable accuracy by the averaged value φ_{exp} at the location of thermocouples T2, T3 and T4. This approximation was therefore used in the interpretation of experimental data. For T1, this method yields an overestimation of about 10–15%, which may be explained by the complex heat transfer phenomena in the convergent channel. It is worth noticing that the numerical results showed a close agreement between the electric power dissipated in the cartridges and the total rate of enthalpy convected by the stream across the channel. The numerical heat losses were limited to a few percent only. It is thought, however, that the model may have slightly underestimated these losses since it considered a simplified two-dimensional geometry.

The numerical Nusselt number distribution may be compared to the reference case of laminar simultaneously thermally and hydraulically developing flow along a two-dimensional channel with symmetrical uniform heat flux surfaces. The calculations of this reference case [31] were found in excellent agreement with the results of Hwang and Fan [35] obtained for $Pr = 0.7$ and 10, reported by Shah and London [36] and fitted by Bejan and Sciubba [37] using empirical formulas of the Churchill–Usagi [38] type. Further calculations were performed for $Pr = 6$, corresponding to the fluid (water) used during experiments. These results may be represented by the following correlation

$$Nu = \frac{\varphi \cdot D_h}{(T_w - T_f)\lambda_f} = [(0.41(x^*)^{-\frac{1}{2}})^2 + 8.235^2]^{\frac{1}{2}} \tag{2}$$

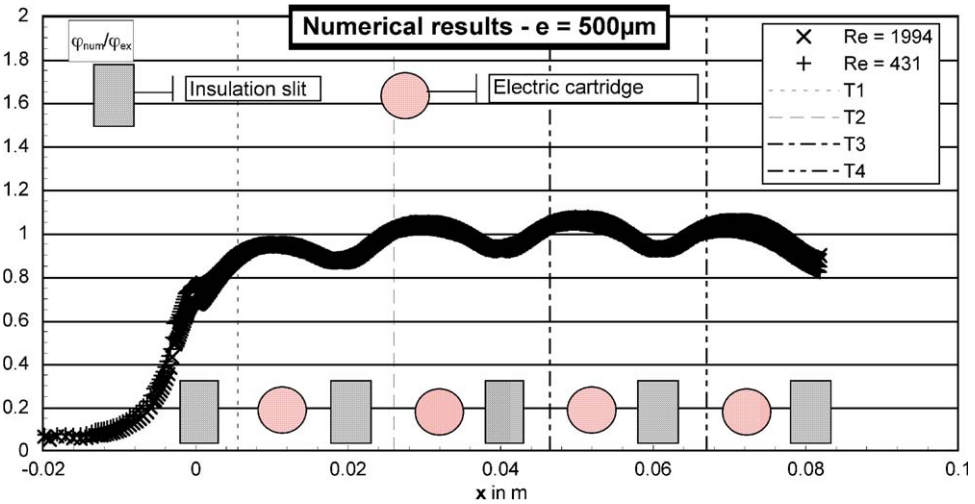

Fig. 2. Distribution of the normalized computed heat flux at the solid/fluid interface for $Re = 1994$ and 431.

where the dimensionless abscissa is

$$x^* = \frac{x}{D_h Re}\frac{1}{Pr} \tag{3}$$

The parameter x^* represents the ratio of the abscissa x to the thermal developing length of a laminar flow in a channel. Eq. (2) assumes uniform inlet velocity and temperature profiles, i.e., it takes into consideration the so-called entrance effect. The Nusselt number was calculated along the channel for six different values of Re ranging between 258 and 1994. The results are presented on Fig. 3 and compared to the uniform inlet law (Eq. (2)). Each of the four groups of data displayed on Fig. 3 corresponds to one of the thermocouple position and varying Reynolds number. Fig. 3 shows a good agreement of the numerical results obtained for the locations of T1–T4 with Eq. (2). Since the velocity and thermal boundary layers are expected to have a finite thickness at channel inlet, it is at first sight surprising that the values obtained for T_1 were not lower than the predictions of Eq. (2). This may be due to overestimation of the actual heat flux by the averaged value φ_{exp} (Fig. 2) and consequently of the Nusselt number.

From this numerical study, which relied on the conventional theory of transport phenomena, it can be concluded that (i) the coupling between convection in the microchannel and longitudinal conduction in the walls is weak in the conditions of this study, (ii) the hypothesis of a uniformly distributed heat flux over the surface of the microchannel is reasonable to estimate the heat transfer coefficient at the solid/fluid interface and (iii) Eq. (2) can be used as a reference curve for the present experimental data to question the conventional laminar theory of transport phenomena.

4. Experimental results

4.1. Heat transfer budget

The knowledge of the experimental heat flux at the fluid/solid interface, namely φ_{exp}, is crucial to the determination of the local Nusselt number. φ_{exp} can be estimated from the total enthalpy rise experienced by the stream between inlet and outlet. The global heat balance for a control volume including the whole test section reads

$$\Phi_{elec} = Q_m Cp_f (T_{out} - T_{in}) - Q_m g \Delta H + \text{thermal losses} \tag{4}$$

where Q_m, g and ΔH, respectively, stand for the mass flow-rate, gravitational acceleration and the head loss in the flow. In Eq. (4), $Q_m g \Delta H$ represents the flow enthalpy rise due to viscous dissipation. This contribution was evaluated using the inlet/outlet pressure losses measurements. The experiments were conducted with a constant total heat flux $\Phi_{elec} = 180$ W and a varying flow-rate. During the experiments, the maximum of $Q_m g \Delta H$ (20 W) was reached for $Re = 8000$ and $e = 400$ μm. If we restrict the discussion to the laminar regime which roughly corresponds to $Re < 3000$, this limit falls to 4 W reached in the $e = 300$ μm channel. In the laminar regime, viscous dissipation can therefore be neglected and the averaged wall heat flux can be inferred from the measured quantities according to

$$\varphi_{exp} \approx \frac{Q_m Cp_f (T_{out} - T_{in})}{2Lw} \tag{5}$$

The thermal losses were evaluated in each experiment by subtracting the enthalpy rise to the electric power dissipated in the blocks. The thermal losses are due to the difference between internal and ambient temperatures, which may be quantified by $T_4 - T_{in}$. Indeed, the inlet

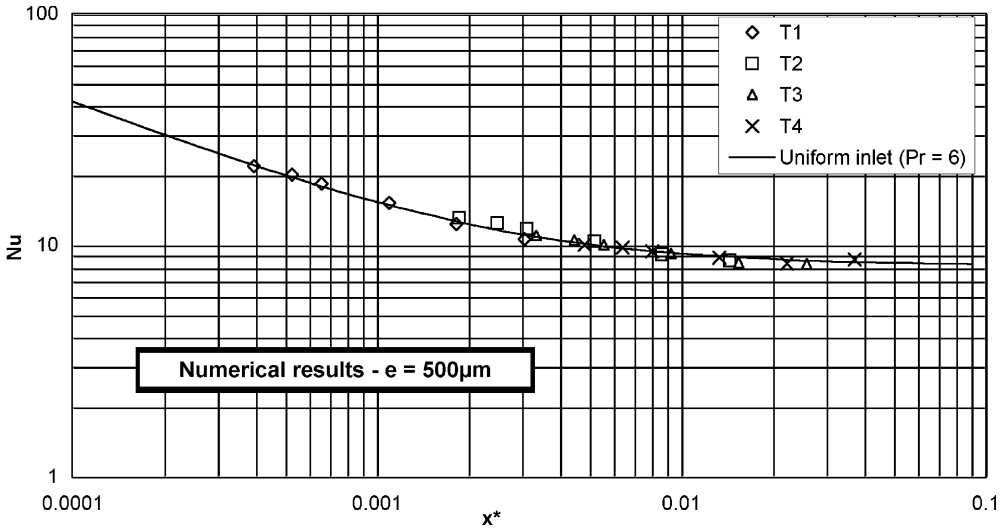

Fig. 3. Variation of the numerical Nusselt number along the channel for $258 < Re < 1994$ and comparison with the uniform inlet law (Eq. (2)).

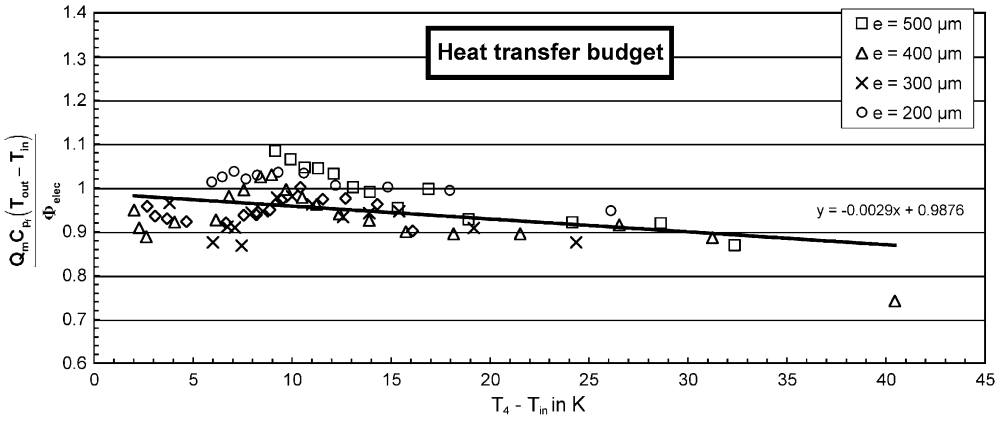

Fig. 4. Heat transfer budget as a function of temperature difference $T_4 - T_{in}$ for $\Phi_{elec} = 180$ W.

temperature T_{in} was maintained close to the room temperature contrary to T_4 which depended on the flow-rate and heating conditions and is representative of the blocks internal temperature field. The enthalpy rise normalized by Φ_{elec} is displayed on Fig. 4 as a function of $T_4 - T_{in}$. It should be noted that this graph was obtained for a single heating power $\Phi_{elec} = 180$ W and several channel spacings. Fig. 4 shows that the thermal losses increase when the flow-rate is decreased giving rise to an increase in the internal temperatures and thus in T_4. Nevertheless, for most cases, thermal losses were lower than 10% so that the heat balance may be considered satisfying. Analysis of the measured data showed that the scatter in Fig. 4 is due to a strong variability in the measurements of T_{out}. The nature of the flow in the exit sump, which is a very thin jet at moderate Reynolds number with a poor quality of mixing, is probably at the origin of this dispersion of results. In order to improve the determination of the heat flux, the enthalpy rise was deduced from the measured heating power by using the linear fit of the data presented on Fig. 4. The averaged heat flux φ_{exp} was then given by Eq. (5).

4.2. Data reduction and error analysis

As already explained, the wall heat flux was considered as uniformly distributed at the microchannel solid/fluid interface and viscous dissipation effects were neglected. Thus, the evolution of the fluid bulk temperature along the channel is given by the linear equation

$$T_f(x) = T_{in} + \frac{2\varphi_{exp} L w}{C p_f Q_m} \frac{x}{L} \tag{6}$$

The heat transfer coefficient (h) and the local Nusselt number (Nu) are computed from the measurements using the following relations

$$h(x) = \frac{\varphi_{exp}}{T_w(x) - T_f(x)} \tag{7}$$

$$Nu(x) = \frac{h(x) D_h}{\lambda_f} \tag{8}$$

where $T_w(x)$ is the solid/fluid interface temperature. For the laminar regime, comparison can be made with Eq. (2) which takes into account the entrance effect. For the hydraulically smooth turbulent regime, the Nusselt number can be compared with the Dittus and Boelter correlation

$$Nu = 0.0243 Re^{0.8} Pr^{0.4} \tag{9}$$

A careful analysis of the experimental uncertainty is critical to the interpretation of data and to the issue of possible deviation from the macroscale theory. In the following expression, the uncertainties on the measured quantities are arranged in decreasing order of importance

$$\left|\frac{\mathrm{d}ANu}{Nu}\right| = \left|\frac{\mathrm{d}(T_w - T_f)}{T_w - T_f}\right| + \left|\frac{\mathrm{d}\varphi_{exp}}{\varphi_{exp}}\right| + \left|\frac{\mathrm{d}(D_h/\lambda)}{D_h/\lambda}\right| \tag{10}$$

For obvious reasons, precise measurements of the interface temperature T_w are extremely difficult in miniaturized setups. Moreover, for given flow conditions and heating rate, $T_w - T_f$ is proportional to the channel spacing e in the macroscale theory. This temperature difference may therefore become very small in microchannels. It should also be noted that $T_w - T_f$ is inversely proportional to the Nusselt number so that large values of Nu due to entrance effects or transition to turbulence lead to higher uncertainties than in a laminar established flow. In the conditions of this study, it can be considered that the uncertainties associated with the determination of $T_w - T_f$, φ_{exp} and D_h/λ are respectively ± 0.2 °C, $\pm 5\%$ and $\pm 5\%$. Fig. 5 displays $\mathrm{d}Nu/Nu = f(Re)$ plots for different channel spacings e and various normalized abscissas x/e corresponding to the limits of the explored ranges during the experiments. $\mathrm{d}Nu/Nu$ was estimated both for laminar developing flows (Eq. (2)) and turbulent fully-developed regimes (Eq. (9)).

4.3. Bias effects on temperature measurements

4.3.1. Raw data

In a first step, the fluid/solid interface temperatures at the abscissa of the thermocouples (T_{1w}–T_{4w}) were assumed to be the raw values given by T1–T4 (see Fig. 1), alike in

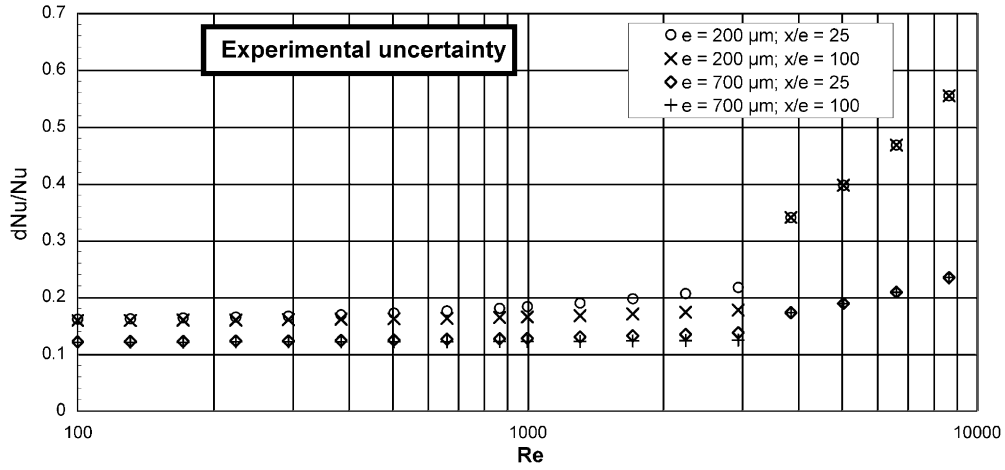

Fig. 5. Uncertainty dNu/Nu for developing laminar flows $100 < Re < 3000$ and fully-developed turbulent flows $3000 < Re < 10000$ ($\Phi_{elec} = 180$ W).

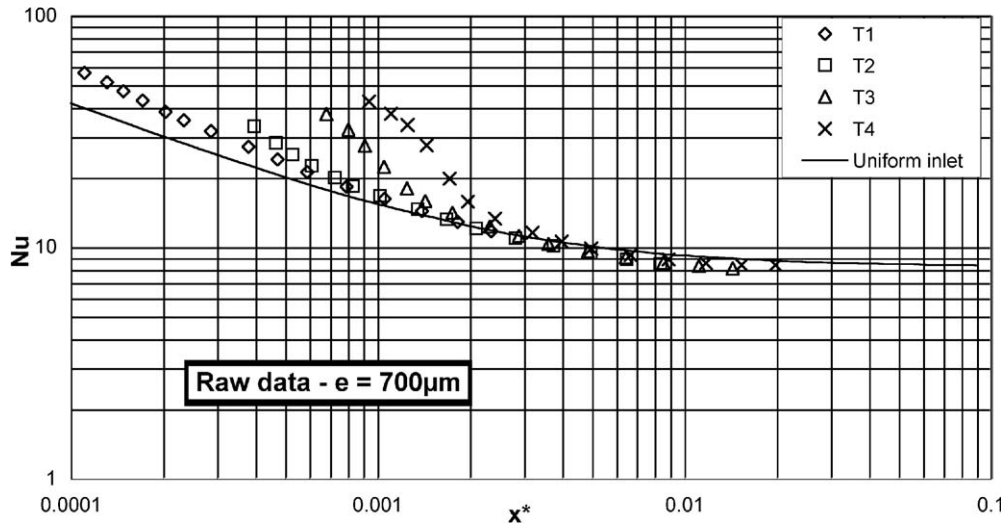

Fig. 6. Variation of Nusselt number along the channel for $e = 700$ µm. The interface wall temperatures were given by T1–T4 without corrections.

the study of Gao et al. [13]. The data obtained in the present work for $e = 700$ µm are presented as $Nu = f(x^*)$ graphs corresponding to $300 < Re < 7500$ (Fig. 6). The results are in good general agreement with the laminar theoretical solution which takes into account the entrance effects (Eq. (2)). However, two kinds of deviations are observed in Fig. 6. Firstly, the experimental points corresponding to thermocouples T2, T3, T4 are significantly upper the theoretical curve for the lowest values of x^*. These conditions correspond to the highest flow-rates used in the experiments. It is worth noting that Nu increases sharply when the Reynolds number exceeds a critical value (see also subsection 4.4.2). This strong enhancement of Nu was already observed by Gao et al. [13] and interpreted by these authors as the result of transition to turbulence. A second type of departure from the theoretical curve occurs when x^* is increased for a given thermocouple, i.e., when the flow-rate is decreased. The experimental values as given by T1–T4 are then slightly lower than the theoretical ones. A similar behavior is also observed for the lowest channel spacings. This effect is obvious on Fig. 7 which presents the evolution of $Nu(x^*)$ at the abscissa of T4, as a function of the channel spacing e. At $x^* = 0.02$ corresponding to laminar fully-developed flow, the reduction in the experimental Nusselt number compared to the uniform inlet conditions law (Eq. (2)) is -12% (-25%) for the channel spacings 700 µm (200 µm). The corresponding values of dNu/Nu at $x^* = 0.02$ is $\pm 12\%$ ($\pm 16\%$) for $e = 700$ µm (200 µm). It follows that the observed diminution in Nu is significant in regard to the experimental uncertainties and the same conclusions can be drawn at the abscissa of T2 and T3. This scale effect on laminar heat transfer in microchannels consisting in a reduction of Nu for decreasing channel spacing was also observed by Gao et al. [13]. However, the reduction in Nu is less in the present study. Gamrat et al. [31] as well as the numerical simulation presented in Section 2 indicate that this scale effect is not due to the coupling between convection in the microchannel and longitudinal conduction in the walls. Interpretation of the measurements is discussed in the following paragraphs.

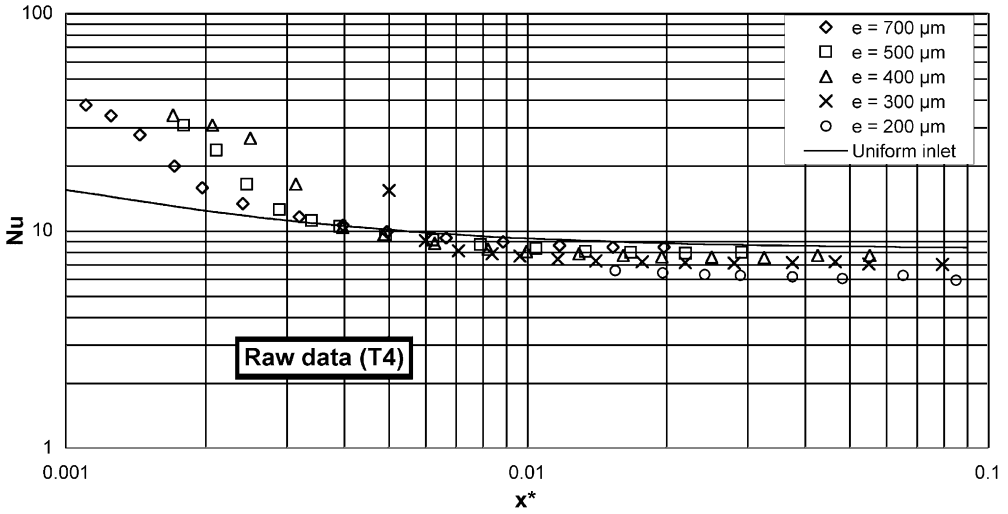

Fig. 7. $Nu(x^*)$ for various channel spacings e. x^* corresponds to the abscissa of T4 ($\Phi_{elec} = 180$ W)—raw data.

4.3.2. Calibration of temperature measurements

It is very difficult to perform precise measurements of interface temperatures in miniaturized arrangements. In the present study, it was chosen to determine the internal temperature of the brass blocks at a short distance from the microchannel surface. Thermocouples were therefore introduced inside the solid body and placed perpendicular to the isotherms. Their sensitive ungrounded junctions were located about 500 µm away from the interface.

Using the values given by T1–T4 for estimating T_{1w} to T_{4w} results in a global error (Michalski et al. [39]) originating from: (i) the deformation of the original temperature field, (ii) the temperature drop across the brass and (iii) the global thermal contact resistance between the thermocouple junction and the brass. Numerical calculations not shown here have suggested that this latter contribution prevails in the global measuring error. However, precise numerical results could not be obtained and hence a direct calibration of the measurement technique was performed in a complementary experiment. This experiment was conducted using three thermocouples inserted in a brass block crossed over by a one-dimensional heat flux. Heat was produced by four heating cartridges and evacuated on the opposite side of the block through a stirred pool filled with melting ice. Two thermocouples (T_{hot}, T_{cold}) were placed in opposite directions perpendicular to the isotherms whereas a third one was parallel to the isotherms as shown in Fig. 8. The distance from T_{hot} or T_{cold} to the horizontal plane containing T_{iso} was set equal to the distance of T1,...,T4 to the microchannel solid/liquid interface. It should be emphasized that the operating conditions were chosen as close as possible to those encountered in the microchannel heat transfer experiments. Moreover, it was verified numerically that the heat flux was uniform near the center of the brass block.

$T_{hot} - T_{iso}$ and $T_{iso} - T_{cold}$ were measured for varying heat flux ranging from 0 to 1.5 W cm^{-2}. This upper limit corresponds to the maximum refrigerating capacity of the

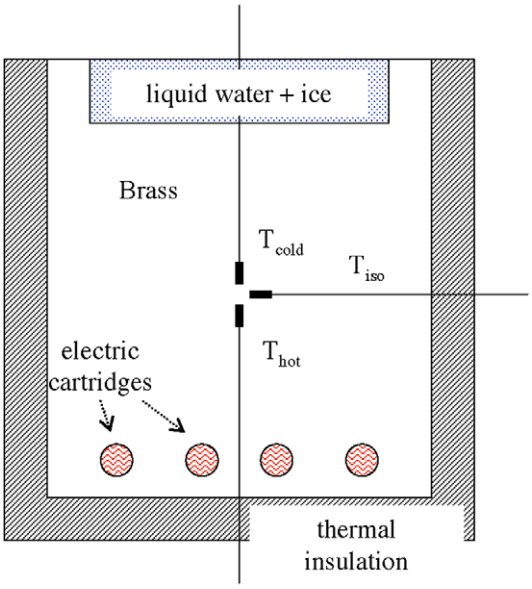

Fig. 8. Sketch of the complementary experimental set-up for the characterization of the temperature measuring error.

pool. Both temperature differences were found to be nearly equal and to vary linearly with the applied heat flux. This can be seen on Fig. 9 which presents the experimental data and a linear fit for $T_{hot} - T_{iso}$. It is enlightening to plot the temperature difference between two points 0.5 mm apart in the brass block (solid line on Fig. 9). This difference is much smaller than $T_{hot} - T_{iso}$ and $T_{iso} - T_{cold}$ which confirms the predominance of the thermal contact resistance in the global measuring error. When extrapolated to the conditions of the microchannel experiments where φ_{exp} reaches 4 Wcm^{-2} for $\Phi_{elec} = 180$ W, the bias effect becomes significant in the microchannel experiments. A correction of the values given by the thermocouples T1–T4 is therefore required to determine more precisely the actual interface temperature. According to the linear fit, this complemen-

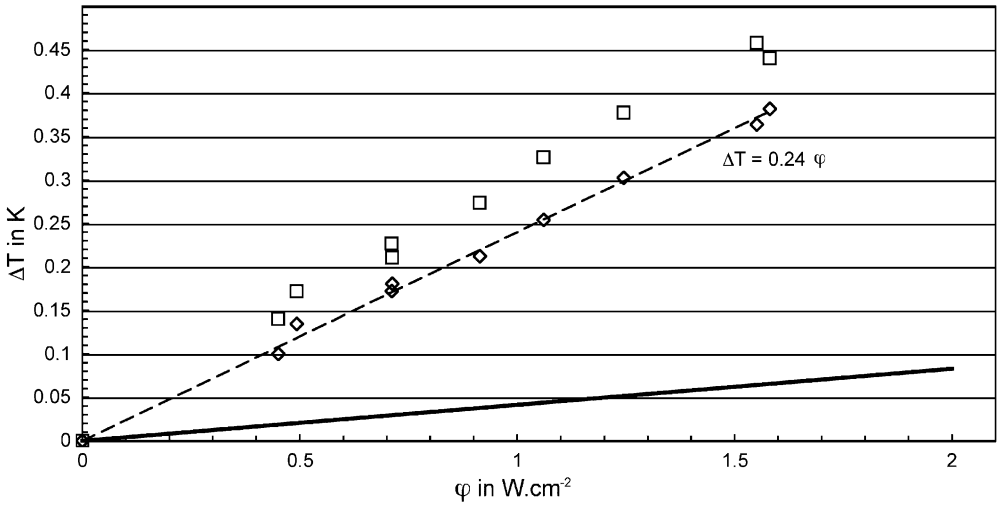

Fig. 9. Temperature measurement error as a function of applied heat flux. □ $T_{iso} - T_{cold}$, ◇ $T_{hot} - T_{iso}$— Pure conduction in brass over 0.5 mm.

tary experiment suggests that the actual wall temperatures at the abscissa of the thermocouple (T_{1w}–T_{4w}) are better estimated by the following equations:

$$\begin{aligned} T_{1w} &= T_1 - 0.24\varphi_{exp} \\ &\vdots \qquad\qquad \vdots \\ T_{4w} &= T_4 - 0.24\varphi_{exp} \end{aligned} \tag{11}$$

where T and φ_{exp} are expressed in K and W cm^{-2}, respectively.

4.4. Results

4.4.1. Friction factor

The Fanning friction factor f was determined from pressure measurements at channel inlet/outlet. It is worth underlining that the two blocks were rounded off in the upstream part so as to form a convergent channel entrance (radius $R = 20$ mm), contrary to several other studies where the channel inlet is characterized by an abrupt contraction. As a consequence, the head losses were neglected in the converging inlet channel. Thus, the pressure at the microchannel entrance was corrected by the inertia term accounting for flow acceleration in the convergent channel and no correction was done on the outlet pressure, as in [13]. f was calculated from the wall shear stress averaged on the wetted perimeter (τ) and the bulk velocity (V_b). It can be linked to the net pressure drop in the microchannel Δp as follows:

$$f = \frac{\tau}{\frac{1}{2}\rho V_b^2} = \frac{\Delta p}{L}\frac{D_h}{2\rho V_b^2} \tag{12}$$

For the fully developed laminar regime Eq. (12) can be written:

$$Po = fRe = 24 \tag{13}$$

where Po is the non-dimensional Poiseuille number. The fully-developed regime hypothesis is valid only after the entrance region. Eq. (13) has therefore to be modified to interpret the results obtained from inlet/outlet pressure measurements. Using $L^+ = L/(ReD_h)$, Shah and London [36] proposed a modified law for the laminar regime:

$$Po(L^+) = \frac{3.44}{\sqrt{L^+}} + \frac{24 + \frac{0.674}{4L^+} - \frac{3.44}{\sqrt{L^+}}}{1 + \frac{2.9^* 10^{-5}}{L^{+2}}} \tag{14}$$

For the hydraulically smooth turbulent regime, comparison can be made with the Blasius law since the extension of the entrance region is about $10D_h$:

$$Po = 0.079Re^{3/4} \tag{15}$$

Fig. 10 shows the Poiseuille number ($Po = fRe$) plotted as a function of the dimensionless channel length $\left(L^+ = \frac{L}{D_h}\frac{1}{Re}\right)$. The present results confirm very well the results of Gao and al. [13] which were obtained in another test section based on the same geometrical design. The experimental Poiseuille number tends to a constant value for sufficiently high values of L^+ where entrance effects are negligible. The classical law of the fully developed laminar regime ($Po = 24$) is found with a very good accuracy for all the tested microchannels. Significant departure from the Shah and London law (Eq. (14)) occurs for the smallest values of L^+, which correspond to the highest flow-rates and therefore to the highest values of the Reynolds number. This is a clear indication of transition to turbulence in the channel.

4.4.2. Heat exchange coefficient

As for pressure losses, the local Nusselt number is plotted as a function of x^* and compared with the uniform inlet reference case (Eq. (2)) for $Pr = 6$ in order to clarify the laminar entrance effects in the heat transfer results. Fig. 11 displays the effect of channel spacing reduction on Nu at the abscissa of T4. The law of the fully developed laminar regime ($x^* > 0.01$) is found with a very good accuracy for all the tested microchannels up to the smallest channel height $e = 200$ μm. The same conclusion could be

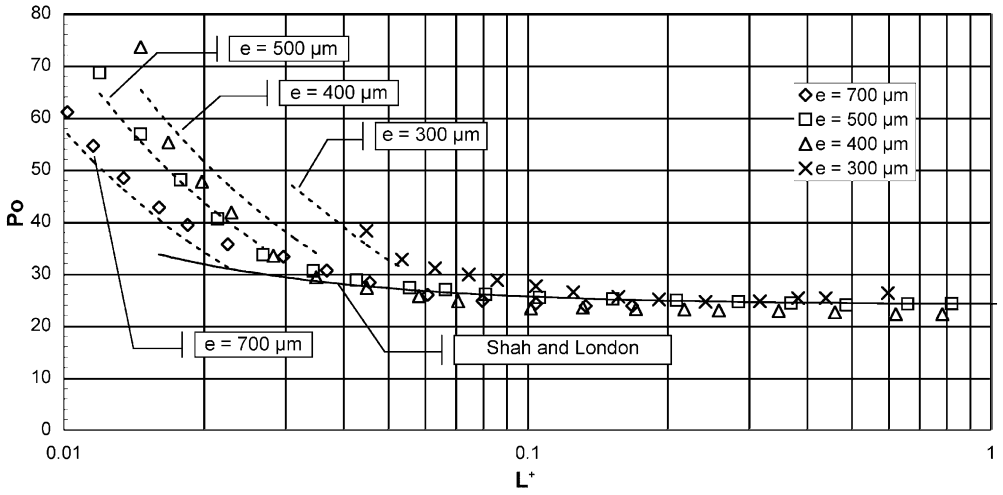

Fig. 10. Poiseuille number as a function of dimensionless channel length $L^+(Re)$—Shah and London [36], - - - - Blasius law.

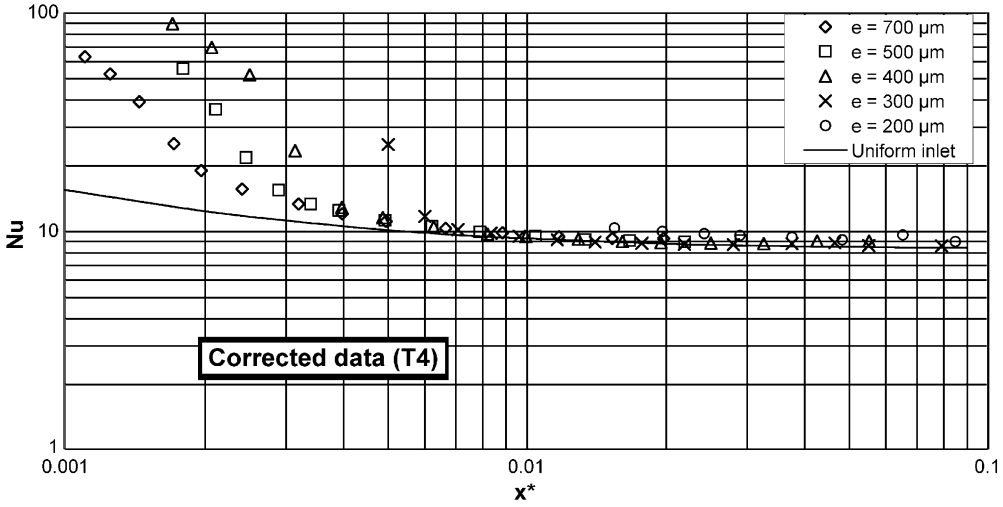

Fig. 11. Evolution of $Nu(x^*)$ as a function of the channel spacing e at the abscissa corresponding to T4 ($\Phi_{elec} = 180$ W)—corrected results.

drawn at the abscissa of T2 and T3. The electric power delivered in the heating cartridges was varied to test the robustness of the correction applied to the measurements. Experiments were carried out for $e = 300$ µm and $\Phi_{elec} = 80$ W, 180 W and 260 W. When the temperature correction was applied (Eq. (11)), the experimental Nusselt number was found to match Eq. (2) for each value of Φ_{elec} (see [32]). This result strongly suggests that the measurement error on the interface temperature is responsible for the Nusselt number reduction observed using the raw data.

The diminution of Nu observed by Gao et al. [13] for channel spacing lower than 500 µm may be tentatively explained by a similar measurement error. Fig. 12 shows the influence of channel spacing on Nu normalized by the value predicted by Eq. (5) both with and without temperature correction. No scale effect appears in the corrected results. It should be noticed that the present data have been corrected using Eq. (11) whereas the values of Gao et al. [13] were recalculated with a more important interface temperature reduction of 2.2 K ($\varphi_{exp} \sim 4$ W cm^{-2} in [13]). This stronger correction originates from the fact that in the experimental set-up used by Gao et al., the walls were composed of bronze which has a lower thermal conductivity than brass, the thermocouples were located further from the interface and the blind holes were probably not completely filled with heat transfer grease.

In sum, the present findings suggest that contrary to previous conclusions, the experimental results match the predictions based on the classical theory of transport phenomena. Its validity in the laminar regime can therefore be extended to the small scales (200 µm) investigated in this work.

Transition to turbulence can better be analyzed using the dimensionless abscissa x/e. The present corrected results are plotted for fixed values of x/e close to 100 on a $Nu(Re)$ graph (Fig. 13). The data clearly depart from the laminar regime law when the Reynolds number of the flow exceeds a critical value Re_c. In order to smooth the

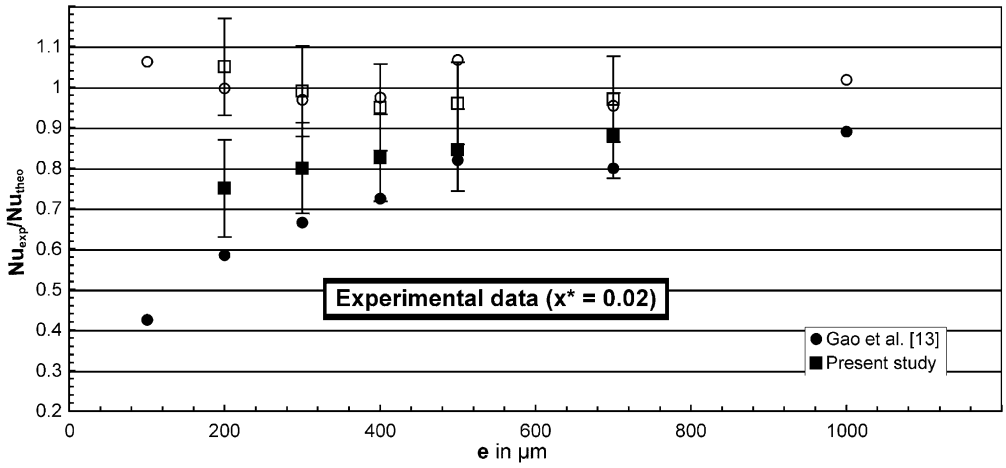

Fig. 12. Effect of the channel spacing on the Nusselt number. Solid symbols: raw data. Open symbols: corrected results.

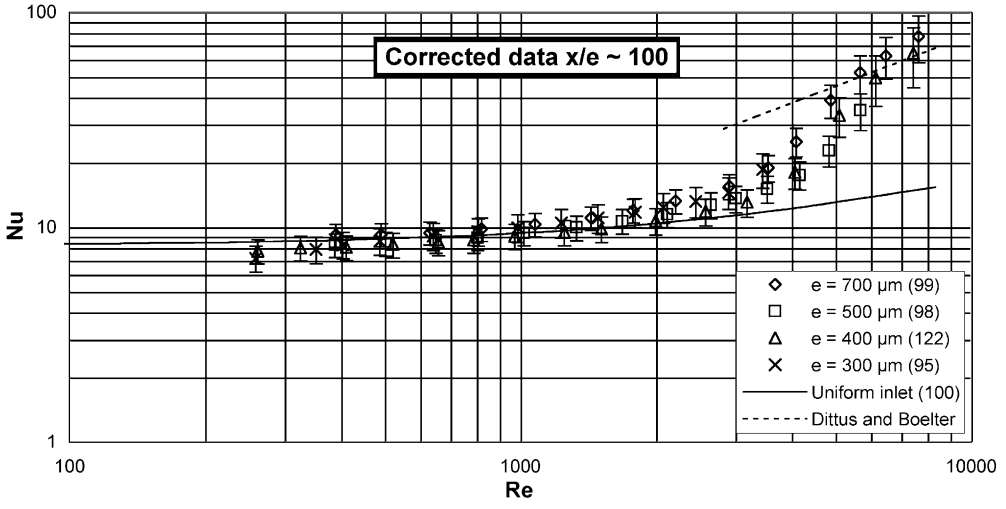

Fig. 13. $Nu(Re)$ plots at $x/e \sim 100$ (exact values indicated in brackets) for different channel spacings.

curves corresponding to the various values of e, it was decided to interpolate the experimental data with a polynomial function of the sixth degree using the least square method. The interpolation curves (not shown here) exhibit a strong curvature in the range $3000 < Re < 5000$ which plausibly corresponds to the onset of turbulence. The Re_c values were therefore estimated at the location of the maximum curvature. The values found for Re_c for the different channel spacing are shown in Table 1. Despite dispersion due to experimental uncertainties, the values found are consistent with the data observed in conventional plane wall channels. Carlson et al. [40] observed transition for $Re \approx 2700$ (note that Re is based on hydraulic diameter and bulk velocity in the present paper). The present observations suggest that the transition to turbulence is not affected by scale effects in these large aspect ratio smooth microchannels. A similar conclusion was reported by Sharp and Adrian [4] who studied transition in microtubes from 50 to 247 μm in diameter with liquids of different polarities. Fig. 13 shows that for $5500 < Re < 8000$, the data do not exhibit any significant scale effect. Beyond Re_c, the present heat transfer results clearly correspond to an intermediate regime where the flow is probably laminar in the upstream part of the channel and exhibits transition somewhere in the channel. The data seem to merge with the Dittus and Boelter correlation for the highest values of Re.

Table 1
Critical Reynolds number Re_c deduced from heat transfer measurements at $x/e \sim 100$

e (in m)	Re_c
700	3500
500	4500
400	3700
300	3400

5. Conclusions

This paper reports on experiments carried out for investigating the hydrodynamics and associated heat transfer of

water flows in two-dimensional rectangular microchannels. The design of the test section enabled variations of the channel spacing between 700 to 200 μm and minimized the longitudinal heat transfer within the walls. In fact, it was demonstrated that the coupling between conduction and convection was weak in the conditions of this study.

At first sight, the present experimental results show a reduction in the Nusselt number for laminar flow at the microscale. Similar observations were already made by Gao et al. [13] but despite a numerical modeling of the experiment [31], their results could not be interpreted. The present findings suggest that a bias effect on the solid/fluid interface temperature measurement may account for the apparent scale effects observed in both studies. Moreover, it can be concluded that in the laminar regime, the validity of the conventional transport phenomena theory may be extended to the small scales (200 μm) investigated in this work.

Transition to turbulence was clearly observed both in the global pressure losses measurements and in the *Nu* vs. *Re* evolutions. Critical Reynolds numbers were found to vary from 3500 to 4500, which is consistent with the values observed at larger scales. Finally, the beginning of the turbulent regime corresponding to $5500 < Re < 8000$ was investigated. In this range, the experimental corrected data matched both the Blasius hydrodynamic law and the Dittus and Boelter heat transfer correlation.

Acknowledgement

This research was supported by the CNRS and Rhône-Alpes region. The fellowship of R. Bavière was supported by the French Ministry of Education and Research, which is gratefully acknowledged. The authors are grateful to Mile Kusulja for the machining of the experimental facilities and wish to thank Gabriel Gamrat for his most valuable contribution to the numerical calculations.

References

[1] D.B. Tuckerman, R.F. Pease, High-performance heat sinking for VLSI, IEEE Electron Dev. Lett. EDL-2, 5 (1981) 126–129.
[2] C.B. Sobhan, S.V. Garimella, A comparative analysis of studies on heat transfer and fluid flow in microchannels, Microscale Therm. Eng. 5 (2001) 293–311.
[3] I. Papautsky, J. Brazzle, T. Ameel, A.B. Frazier, Laminar fluid behavior in microchannels using micropolar fluid theory, Sensor. Actuat. A 73 (1999) 101–108.
[4] K.V. Sharp, R.J. Adrian, Transition from laminar to turbulent flow in liquid filled microtubes, Exp. Fluids 36 (2004) 741–747.
[5] Z.X. Li, D.X. Du, Z.Y. Guo, Experimental study on flow characteristics of liquid in circular microtubes, Microscale Therm. Eng. 7 (2003) 253–265.
[6] D.J. Phares, G.T. Smedley, A study of laminar flow of polar liquids through circular microtubes, Phys. Fluids 16 (2004) 1267–1272.
[7] J. Judy, D. Maynes, B.W. Webb, Characterization of frictional pressure drop for liquid flows through microchannels, Int. J. Heat Mass Transfer 45 (2002) 3477–3489.
[8] M.J. Kohl, S.I. Abdel-Khalik, S.M. Jeter, D.L. Sadowski, An experimental investigation of microchannel flow with internal pressure measurements, Int. J. Heat Mass Transfer 48 (2005) 1518–1533.
[9] R. Bavière, F. Ayela, S. Le Person, M. Favre-Marinet, Experimental characterization of water flow through smooth rectangular microchannels, Phys. Fluids 17 (9) (2005) 098105 1–098105 4.
[10] X.F. Peng, G.P. Peterson, B.X. Wang, Heat transfer characteristics of water flowing through microchannels, Exp. Heat Transfer 7 (1994) 265–283.
[11] W. Qu, Gh.M. Mala, D. Li, Heat transfer for water flow in trapezoidal silicon microchannels, Int. J. Heat Mass Transfer 43 (2000) 3925–3936.
[12] G.P. Celata, M. Cumo, M. Guglielmi, G. Zummo, Experimental investigation of hydraulic and single-phase heat transfer in 0.130-mm capillary tube, Microscale Therm. Eng. 6 (2002) 85–97.
[13] P. Gao, S. Le Person, M. Favre-Marinet, Scale effects on hydrodynamics and heat transfer in two-dimensional mini and microchannels, Int. J. Therm. Sci. 41 (2002) 1017–1027.
[14] H.Y. Wu, Ping Cheng, An experimental study of convective heat transfer in silicon microchannels with different surface conditions, Int. J. Heat Mass Transfer 46 (2003) 2547–2556.
[15] S. Reynaud, F. Debray, J.-P. Franc, T. Maitre, Hydrodynamics and heat transfer in two-dimensional minichannels, Int. J. Heat Mass Transfer 48 (2005) 3197–3211.
[16] C.P. Tso, S.P. Mahulikar, Experimental verification of the role of Brinkman number in microchannels using local parameters, Int. J. Heat Mass Transfer 43 (10) (2000) 1837–1849.
[17] A. Weisberg, H.H. Bau, J.N. Zemel, Analysis of micro-channels for integrated cooling, Int. J. Heat Mass Transfer 35 (1992) 2465–2474.
[18] K.C. Toh, X.Y. Chen, J.C. Chai, Numerical computation of fluid flow and heat transfer in micro-channels, Int. J. Heat Mass Transfer 45 (2002) 5133–5141.
[19] J. Li, G.P. Peterson, P. Cheng, Three-dimensional analysis of heat transfer in a micro-heat sink with single phase flow, Int. J. Heat Mass Transfer 47 (2004) 4215–4231.
[20] A.G. Fedorov, R. Viskanta, Three-dimensional conjugate heat transfer in the micro-channel heat sink for electronic packaging, Int. J. Heat Mass Transfer 43 (2000) 399–415.
[21] W. Qu, I. Mudawar, Analysis of three-dimensional heat transfer in micro-channel heat sinks, Int. J. Heat Mass Transfer 45 (2002) 3973–3985.
[22] H. Herwig, O. Hausner, Critical view on "new results in micro-fluid mechanics": an example, Int. J. Heat Mass Transfer 46 (2003) 935–937.
[23] W. Qu, I. Mudawar, Experimental and numerical study of pressure drop and heat transfer in a single–phase micro-channel heat sinks, Int. J. Heat Mass Transfer 45 (2002) 2549–2565.
[24] I. Tiselj, G. Hetsroni, B. Mavko, A. Mosyak, E. Pogrebnyak, Z. Segal, Effect of axial conduction on the heat transfer in microchannels, Int. J. Heat Mass Transfer 47 (2004) 2551–2565.
[25] D. Lelea, S. Nishio, K. Takano, The experimental research on microtube heat transfer and fluid flow of distilled water, Int. J. Heat Mass Transfer 47 (2004) 2817–2830.
[26] P.S. Lee, S.V. Garimella, D. Liu, Investigation of heat transfer in rectangular microchannels, Int. J. Heat Mass Transfer 48 (2005) 1688–1704.
[27] Z.Y. Guo, Z.X. Li, Size effect on microscale single-phase flow and heat transfer, Int. J. Heat Mass Transfer 46 (2003) 149–159.
[28] R.B. Peterson, Numerical modeling of conduction effects in microscale counterflow heat exchangers, Microscale Therm. Eng. 3 (1999) 17–30.
[29] G. Maranzana, I. Perry, D. Maillet, Mini-and micro-channels: influence of axial conduction in the walls, Int. J. Heat Mass Transfer 47 (2004) 3993–4004.
[30] C.J. Kroeker, H.M. Soliman, S.J. Ormiston, Three-dimensional thermal analysis of heat sinks with circular cooling micro-channels, Int. J. Heat Mass Transfer 47 (22) (2004) 4733–4744.
[31] G. Gamrat, M. Favre-Marinet, D. Asendrych, Conduction and entrance effects on laminar liquid flow and heat transfer in rectan-

gular microchannels, Int. J. Heat Mass Transfer 48 (14) (2005) 2943–2954.
[32] R. Bavière, Etude de l'Hydrodynamique et des Transferts de Chaleur dans des Microcanaux, PhD thesis, University of Grenoble I, 2005, http://tel.ccsd.cnrs.fr/.
[33] A. Bejan, Convection Heat Transfer, second ed., John Wiley and Sons, New York, USA, 1995.
[34] G. Gamrat, Numerical modeling of heat transfer in microchannels, Msc report, University of Czestochowa, Poland, 2003.
[35] C.L. Hwang, L.T. Fan, Finite difference analysis of forced-convection heat transfer in entrance region of a flat rectangular duct, Appl. Sci. Res. 13 (1964) 401–422.
[36] R.K. Shah, A.L. London, Laminar flow forced convection in ductsAdvanced Heat Transfer, Academic Press, New York, 1978, ch. 6.
[37] A. Bejan, E. Sciubba, The optimal spacing of parallel plates cooled by forced convection, Int. J. Heat Mass Transfer 35 (1992) 3259–3264.
[38] S.W. Churchill, R. Usagi, A general expression for the correlation of rates of transfer and other phenomena, A. I. Ch. E. J. 18 (1972) 1121–1128.
[39] L. Michalski, K. Eckersdorf, J. Kucharski, J. McGhee, Temperature measurement, second ed., John Wiley and Sons, Chichester, 2001.
[40] D.R. Carlson, S.E. Widnall, M.F. Peeters, A flow-visualization study of transition in plane Poiseuille flow, J. Fluid Mech. 121 (1982) 487–505.